Comparison of the dynamic performance of nonlinear one and two degree-of-freedom vibration isolators with quasi-zero-stiffness

Yong Wang[1,2*], Shunming Li[1], Simon A. Neild[2], Jason Zheng Jiang[2]

[1]*College of Energy and Power Engineering, Nanjing University of Aeronautics and Astronautics, Nanjing 210016, China.*

[2]*Department of Mechanical Engineering, Queen's Building, University of Bristol, Bristol BS8 1TR, UK.*

*Corresponding author. Phone:+86 15951897282.

E-mail: wangy1921@126.com.

Abstract

Nonlinear stiffness isolation mounts, which offer a high static stiffness alongside a low dynamic stiffness or even quasi-zero-stiffness (QZS) over a displacement range have been proposed. These vibration isolators offer a higher isolation frequency band of low transmissibility than conventional linear devices. Here, three kinds of nonlinear two degree-of-freedom (DOF) vibration isolators with QZS characteristic are analysed in order to further improve the isolation performance. The dynamic response is obtained using the Harmonic Balance Method (HBM) and the peak dynamic displacement is obtained using backbone curve analysis and energy balancing method. The optimum isolation performance of the nonlinear 2DOF vibration isolators are evaluated for four performance indexes and compared with three baseline vibration isolators. These are a linear and a QZS 1DOF vibration isolator as well as a linear 2DOF vibration isolator. To ensure a fair comparison, the static displacement of each vibration isolator is kept constant. The comparison demonstrates that a nonlinear 2DOF vibration isolator can be tuned to achieve a better isolation performance in the higher isolation frequency band than the baseline vibration isolators, while retaining a moderate peak dynamic displacement and peak transmissibility. In addition, the best vibration isolator is identified for each of the four performance indexes.

Keywords: Nonlinear vibration isolator; Two degree-of-freedom; Quasi-zero-stiffness; Dynamic analysis; Performance analysis.

1 Introduction

The vibration isolator is a device placed between a vibration source such as an engine and a structure needing protection from this source [1, 2] and is widely used in the engineering industry. Since a linear vibration isolator can provide an effective isolation when the excitation frequencies are greater than $\sqrt{2}\omega_n$, where ω_n is the natural frequency of the system, the two most important characteristics of a linear vibration isolator are the natural frequency and load bearing capacity. As is well known, for a linear vibration isolator, there is a compromise between these two characteristics, namely the desire to minimize ω_n (and so maximize the isolation frequency band) while also retaining a reasonable load bearing capacity, which is partially governed by keeping the static displacement, and hence the vertical stiffness, at an acceptable level. Without increasing the supported weight, this vertical stiffness is the only parameter to reduce the natural frequency. This compromise can be improved by introducing a nonlinear stiffness element to the vibration isolator, hence achieving a quasi-zero-stiffness (QZS) characteristic. The QZS vibration isolator is usually composed of a load bearing elastic element with positive stiffness and a novel mechanism that provides negative stiffness over a small displacement range reducing the natural frequency. The load bearing elastic element is usually a vertical spring, and at the static equilibrium position, this positive stiffness is exactly balanced by the nonlinear negative stiffness mechanism. This results in zero stiffness at the static equilibrium position and low dynamic stiffness over a dynamic displacement range, which is assumed to be smaller than the static displacement. Through this arrangement, a lower natural frequency and hence a larger isolation frequency band can be achieved than with a linear vibration isolator.

One degree-of-freedom (DOF) QZS vibration isolators have attracted much attention. Alabudzev *et al.* [3] proposed many different kinds of QZS vibration isolators and summarized their technical design methods and practical applications. Carrella *et al.* [4, 5] proposed a QZS vibration isolator composed of a vertical spring acting in parallel with two inclined springs, used to provide the negative stiffness mechanism, and studied the static and dynamic behaviors theoretically. Xu *et al.* [6] also tested this kind of QZS vibration isolator and verified that the QZS vibration isolator can provide better isolation performance than the linear counterpart. Le and Ahn [7, 8] designed a QZS vibration isolator composed of a positive stiffness structure and two symmetric negative stiffness structures for improving isolation of the vehicle seat under low excitation frequencies, and designed controllers to further improve the performance [9]. Other negative stiffness mechanisms considered include axial loaded bars [10, 11], buckled beams [12, 13], a bistable composite plate [14, 15], novel planar springs [16], a cam-roller-spring mechanism [17, 18], a scissor-like structure [19], and magnets or electromagnets devices [20-22]. Also several researchers have considered the effects of stiffness and load

imperfections [23-26] on the performance of the QZS vibration isolator, they all showed that the QZS vibration isolator can still perform better than the linear counterpart when the excitation amplitude is not too large. For the small excitation amplitude, the 1DOF QZS vibration isolator can achieve a lower natural frequency, a larger isolation frequency band and a smaller peak transmissibility than the linear counterpart, while retaining the load bearing capacity.

For the 1DOF vibration isolator, the force or displacement transmissibility reduces at a rate of 40dB/decade in the isolation frequency band. This can be doubled by using a 2DOF vibration isolator. Although the structure of 2DOF vibration isolator is more complicated, with an additional mass, spring and damper, it is used in some practical applications [27, 28]. Lu *et al.* [29, 30] proposed two kinds of nonlinear 2DOF vibration isolators with QZS characteristic and studied the force or displacement transmissibility theoretically. Compared with the linear 2DOF vibration isolator, they found the nonlinear 2DOF vibration isolator has superior isolation performance in the higher isolation frequency band.

Building on the work by Lu *et al.*, in this paper we conduct a comparative study of three kinds of nonlinear 2DOF vibration isolators, benchmarking their isolation performance against the more established 1DOF QZS vibration isolator and linear 1 and 2DOF vibration isolators. For vibration isolators, the static displacement should be limited for a realistic design, so in order to ensure a fair comparison, the static displacement of each vibration isolator is held constant. While imposing this constraint on the isolation performance, the six vibration isolators are tuned for four different performance indexes. These are:

(1) Peak dynamic displacement;

(2) Peak transmissibility;

(3) Unity isolation frequency band, the frequency band in which the transmissibility amplitude is less than unity;

(4) -40dB isolation frequency band, the frequency band in which the transmissibility amplitude is less than 0.01 (This is the performance index used by Lu *et al.*).

This first two performance indexes have been included as they capture the worst case displacements and forces transmitted to the device being isolated. The third one gives an indication of the frequency band at which the vibration isolator starts to have a beneficial effect and the fourth one gives an indication of the frequency band at which the force transmitted to the device is cut to 1% of the exciting force. This paper investigates whether the nonlinear 2DOF vibration isolator can achieve a better isolation performance in the higher isolation frequency band, also have a smaller peak transmissibility and a larger unity isolation frequency band, while keeping the peak dynamic displacement moderate. This paper also considers structural parameter sets for the nonlinear 2DOF vibration isolators and gives guidance in choosing the best linear or nonlinear, 1 or 2DOF

vibration isolator according to the four performance indexes.

The organization of this paper is as follows. In Section 2, a brief description of a typical 1DOF QZS vibration isolator is presented and its dynamic response and isolation performance are compared with the linear counterpart. In Section 3, the dynamic response and isolation performance of the linear 1DOF and 2DOF vibration isolators are compared. In Section 4, three nonlinear 2DOF vibration isolators are presented, the dynamic equations are established and the Harmonic Balance Method (HBM) is used to obtain the dynamic response. The peak dynamic displacement is obtained using backbone curve analysis and energy balancing method. The best structural parameter sets are found based on the four performance indexes and the isolation performance of the nonlinear 2DOF vibration isolators are compared. In Section 5, the most suitable linear or nonlinear, 1 or 2DOF vibration isolators according to the four performance indexes are discussed. Conclusions are drawn in Section 6.

2 The 1DOF QZS vibration isolator

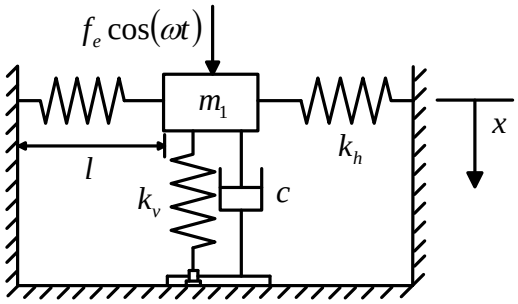

Fig. 1 Model of a 1DOF QZS vibration isolator at the static equilibrium position.

A typical 1DOF QZS vibration isolator composed of vertical spring used as load bearing element and lateral springs used as negative stiffness mechanism is shown in Fig. 1. The vertical spring deflection adjustment device is used to ensure that the mass m_1 is balanced at the static equilibrium position and the lateral springs are in the horizontal position. This arrangement can accommodate changes in the mass m_1, which is a little different from the structure described in [4-6], but is in line with practical implementations, such as [15, 16]. The stiffness of the vertical and lateral springs are k_v and k_h; the initial length of the lateral springs is l_0 and the length when they are compressed in the horizontal position, the static equilibrium position, is *l*; the damping coefficient of the damper is *c*; x is the displacement of the mass m_1 from the static equilibrium position and the mass m_1 is excited with a harmonic force $f_e\cos(\omega t)$.

The nonlinear force-displacement relationship for the 1DOF QZS vibration isolator shown in Fig. 1 is given as

$$f = k_v x + 2k_h x\left(1-\frac{l_0}{\sqrt{x^2+l^2}}\right), \tag{1}$$

and in non-dimensional form as

$$F = X + 2KX\left(1 - \frac{U}{\sqrt{X^2 + (UL)^2}}\right), \tag{2}$$

by using

$$X = \frac{x}{x_s},\quad F = \frac{f}{k_v x_s},\quad U = \frac{l_0}{x_s},\quad L = \frac{l}{l_0},\quad K = \frac{k_h}{k_v}. \tag{3}$$

Here x_s is the static equilibrium displacement of the 1DOF QZS vibration isolator and is arguably best thought of the vertical spring k_v must be compressed at the static equilibrium position to support the mass m_1, hence $x_s = m_1 g / k_v$. Note that this means the non-dimensional force may be written as $F = f/(m_1 g)$.

Using Eq. (2), the gradient of the non-dimensional force-displacement relationship at the static equilibrium position ($X = 0$) is

$$\left.\frac{dF}{dX}\right|_{X=0} = 1 + 2K\left(1 - \frac{1}{L}\right). \tag{4}$$

By definition, a 1DOF QZS vibration isolator has zero effective stiffness at the static equilibrium position, using Eq. (4), this places the condition on the static equilibrium position that the length ratio for the lateral spring is given by

$$L = \frac{2K}{1 + 2K}. \tag{5}$$

The non-dimensional force-displacement curves of the 1DOF QZS vibration isolator for various values of U and L when $K = 1$ are shown in Fig. 2. When $K = 1$ and $L = 2/3$, the QZS characteristic is obtained, as U increases, both the dynamic force and effective stiffness decrease, and the displacement range which is smaller than the effective stiffness of the linear counterpart increases, however this is at the cost of a wider mount ($L = l/l_0$ is fixed and $U = l_0/x_s$ increases). When $K = 1$ and $U = 2$, as L increases, both the dynamic force and effective stiffness increase, and the displacement range which is smaller than the effective stiffness of the linear counterpart reduces.

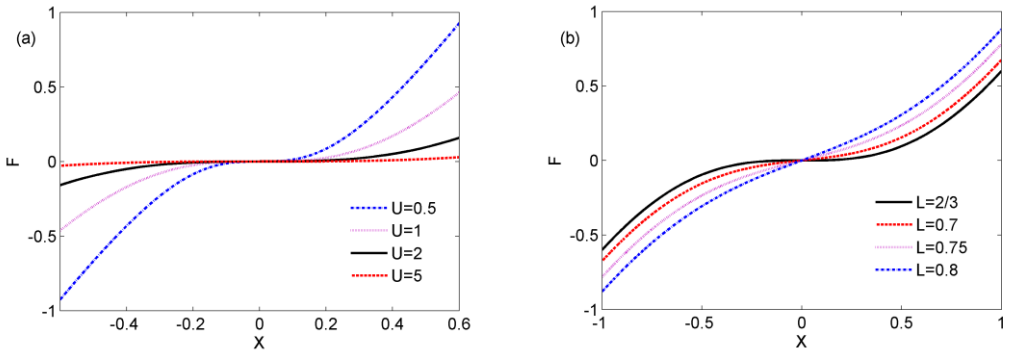

Fig. 2. Non-dimensional force-displacement curves for the 1DOF QZS vibration isolator with (a) different U when $K = 1$ and $L = 2/3$, (b) different L when $K = 1$ and $U = 2$.

When the amplitude of the displacement is small, the non-dimensional force can be expanded as a Taylor series expansion at the static equilibrium position, $X = 0$, to give

$$F \cong \alpha X + \gamma X^3, \qquad \alpha = 1 - 2K\frac{1-L}{L}, \qquad \gamma = \frac{K}{U^2 L^3}. \tag{6}$$

Note here we keep a linear stiffness term for generality, but we note that for a 1DOF QZS vibration isolator, $\alpha = 0$. The dynamic equation of the 1DOF QZS vibration isolator under force excitation using a Taylor series expansion is given as

$$m_1\ddot{x} + c\dot{x} + k_v\alpha x + k_v\gamma\frac{x^3}{x_s^2} = f_e\cos(\omega t), \tag{7}$$

where the dots denote derivatives with respect to time *t*. Eq. (7) can be written in non-dimensional form as

$$X'' + 2\zeta X' + \alpha X + \gamma X^3 = F_e\cos(\Omega T), \tag{8}$$

where Eq. (3) is used along with

$$\frac{k_v}{m_1} = \omega_n^2, \quad \frac{c}{m_1} = 2\zeta\omega_n, \quad \Omega = \frac{\omega}{\omega_n}, \quad T = \omega_n t, \quad (\cdot)' = \frac{d(\cdot)}{dT}. \tag{9}$$

To analyse the steady state response of the 1DOF QZS vibration isolator, the HBM is used. Assuming an approximate solution of the form $X(T) = X_m\cos(\Omega T + \Phi)$, the resulting amplitude-frequency relationship is

$$\left(\alpha X_m - \Omega^2 X_m + \frac{3}{4}\gamma X_m^3\right)^2 + (2\zeta\Omega X_m)^2 = F_e^2. \tag{10}$$

The backbone curve describes the peak dynamic displacement of the vibration system which is undamped and unforced and the excitation frequencies at which they occur [31]. The peak dynamic displacement of the forced, damped system corresponds closely with the point where the response crosses the backbone curve [31]. This crossing point occurs when the response is in quadrature with the forcing, such that the forcing input matches the damping. Hence, Eq. (10), at this point, may be written as

$$\Omega_b^2 = \alpha + \frac{3}{4}\gamma X_{mp}^2, \qquad X_{mp} = \frac{F_e}{2\zeta\Omega_b}. \tag{11}$$

So the backbone curve and peak dynamic displacement of the 1DOF QZS vibration isolator are obtained. Likewise, the force transmitted to the base through the 1DOF QZS vibration isolator is given as $F_t = 2\zeta X' + \alpha X + \gamma X^3$, from which, the force transmissibility can be obtained as

$$G_{FN} = \frac{\sqrt{\left(\alpha X_m + \frac{3}{4}\gamma X_m^3\right)^2 + (2\zeta\Omega X_m)^2}}{F_e}. \tag{12}$$

Using Eq. (10), Eq. (12) can also be written as

$$G_{FN} = \frac{\sqrt{\left(\alpha + \frac{3}{4}\gamma X_m^2\right)^2 + (2\zeta\Omega)^2}}{\sqrt{\left(\alpha - \Omega^2 + \frac{3}{4}\gamma X_m^2\right)^2 + (2\zeta\Omega)^2}}. \tag{13}$$

It is of interest to compare the force transmissibility of the 1DOF QZS vibration isolator with an equivalent linear one with the same load bearing capacity. Since the 1DOF QZS vibration isolator is composed of load bearing element and negative stiffness mechanisms, the equivalent linear 1DOF vibration isolator is achieved by removing the negative stiffness mechanisms, such that $\alpha = 1$ and $\gamma = 0$. This satisfies the requirement that the static displacement of both vibration isolators is the same. Hence, the force transmissibility of the equivalent linear 1DOF vibration isolator is given as

$$G_{FL} = \sqrt{\frac{1+(2\zeta\Omega)^2}{\left(1-\Omega^2\right)^2+(2\zeta\Omega)^2}}\,. \tag{14}$$

The peak dynamic displacement, peak force transmissibility, unity isolation frequency band and -40dB isolation frequency band are used to evaluate the isolation performance of the vibration isolator. The isolation performance of the 1DOF QZS vibration isolator depends on the excitation force amplitude and damping ratio. From previous studies, it is understandable that if the excitation force amplitude is very large or the damping ratio is very small, the resonant frequency of the 1DOF QZS vibration isolator can exceed the natural frequency of its linear counterpart and the isolation performance can be worse. For the present study, we consider a small excitation force case with a damping ratio of $\zeta = 0.05$.

The dynamic response and force transmissibility of the 1DOF QZS vibration isolator for different U are shown in Fig. 3, using Eq. (10) and Eq. (12) respectively. The corresponding curves for the linear 1DOF vibration isolator are plotted in the same figure for comparison. Fig. 3 and subsequent plots also show the backbone curves as dotted lines and the peak dynamic displacement and peak force transmissibility points are shown as circles.

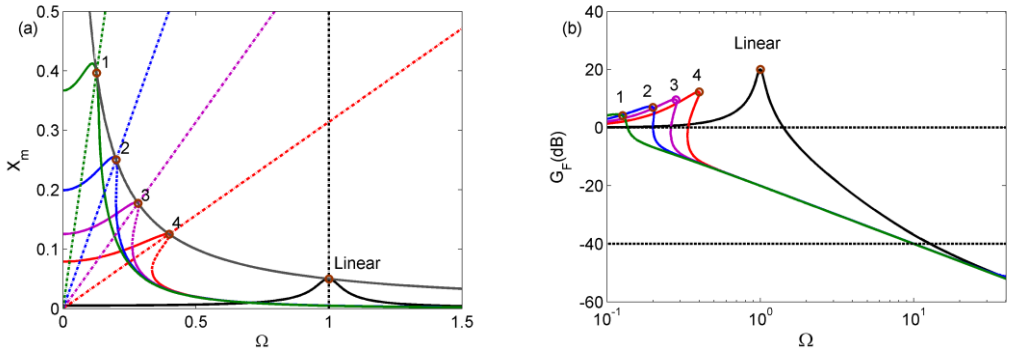

Fig. 3 (a) Dynamic response and (b) force transmissibility of the 1DOF QZS vibration isolator for different U with $K = 1$, $L = L_{QZS} = 2/3$, $\zeta = 0.05$ and $F_e = 0.005$. Curve 1: $U = 5$; Curve 2: $U = 2$; Curve 3: $U = 1$; Curve 4: $U = 0.5$.

It can be seen that for the 1DOF QZS vibration isolator, when $K = 1$ and $L = 2/3$, the QZS characteristic is obtained as the backbone curves start at zero frequency. As

$U = l_0 / x_s$ increases, which results in a reduction of the nonlinear stiffness term γ, see Eq. (6), the peak force transmissibility decreases, but at the cost of an increased peak dynamic displacement. The unity isolation frequency band increases while the -40dB isolation frequency band is relatively insensitive to this change. Note that the peak dynamic displacement is proportional to Ω_b^{-1} and the peak force transmissibility has an approximately linear relationship with Ω_b. This can be seen by substituting Eq. (11) into Eq. (12) to give an approximate peak force transmissibility of $\Omega_b/(2\zeta)$ when the damping ratio ζ is small. When K and U are fixed, the dynamic response and force transmissibility of the 1DOF QZS vibration isolator for different L are studied in detail in [5], so this is not shown here. In the following section, when investigating the isolation performance of the nonlinear 2DOF vibration isolator, $U = 2$ is selected as a reasonable compromise between the four performance indexes.

In summary, the 1DOF QZS vibration isolator can have a smaller peak force transmissibility and a larger isolation frequency band. In the higher isolation frequency band, where the dynamic displacement is small, and the nonlinear stiffness effects can be neglected, so as with the 1DOF linear vibration isolator, the force transmissibility reduces at a rate of 40dB/decade. This can be improved by using the 2DOF vibration isolator, whose force transmissibility reduces at a rate of 80dB/decade in the higher isolation frequency band. The next section analyses the dynamic response and force transmissibility of the linear 2DOF vibration isolator, before moving on to nonlinear 2DOF vibration isolators in Section 4.

3 The linear 2DOF vibration isolator

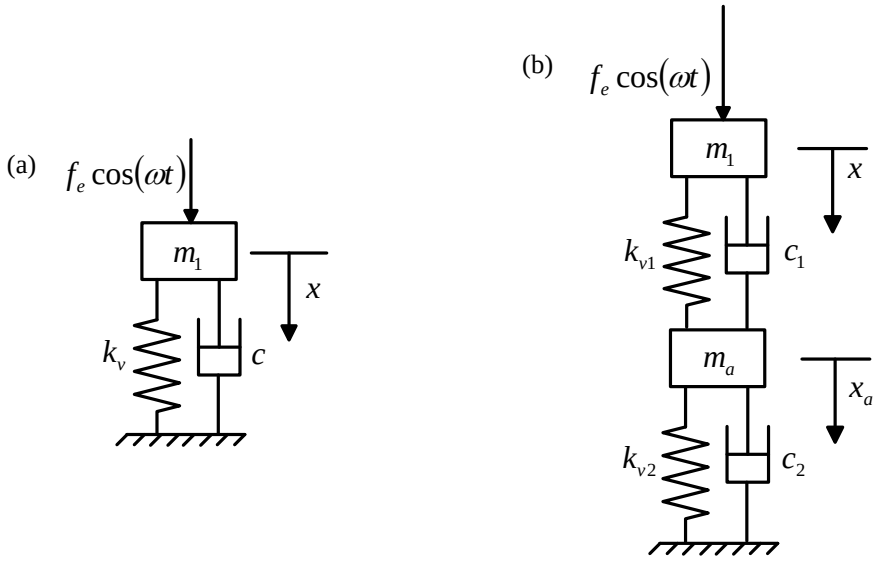

Fig. 4 Linear (a) 1DOF and (b) 2DOF vibration isolators at the static equilibrium position.

The linear 1DOF and 2DOF vibration isolators are presented in Fig. 4, where the

parameters and states for the linear 2DOF vibration isolator are also defined. As discussed in the Introduction, the static displacement of different vibration isolators is set to be the same. This results in the requirement that the static displacement of both linear vibration isolators equals $m_1 g / k_v$. Based on this and by using mass ratio $\sigma = m_a / m_1$, stiffness ratio $k_{v1} / k_v = v$ and $k_{v2} / k_v = \beta$, the following equation can be obtained

$$v = \frac{\beta}{\beta - (1+\sigma)}. \tag{15}$$

Using Eq. (15), the dynamic equations for both linear vibration isolators at the static equilibrium position can be written in non-dimensional form as

1DOF: $$X'' + 2\zeta X' + X = F_e \cos(\Omega\tau), \tag{16a}$$

2DOF: $$\begin{bmatrix} 1 & 0 \\ 0 & \sigma \end{bmatrix}\begin{pmatrix} X'' \\ X_a'' \end{pmatrix} + \begin{bmatrix} 2\zeta_1 & -2\zeta_1 \\ -2\zeta_1 & 2\zeta_1 + 2\sigma\zeta_2 \end{bmatrix}\begin{pmatrix} X' \\ X_a' \end{pmatrix} + \begin{bmatrix} v & -v \\ -v & v+\beta \end{bmatrix}\begin{pmatrix} X \\ X_a \end{pmatrix} = \begin{bmatrix} F_e \cos(\Omega T) \\ 0 \end{bmatrix}, \tag{16b}$$

where the non-dimensional parameters are defined in Eq. (3), Eq. (9) and

$$\frac{x_a}{x_s} = X_a, \quad \frac{c_1}{m_1} = 2\zeta_1 w_n, \quad \frac{c_2}{m_a} = 2\zeta_2 w_n. \tag{17}$$

Denoting the solutions to Eq. (16) in the forms

$$X(T) = X_m \cos(\Omega T + \Phi), \tag{18a}$$

$$\begin{pmatrix} X(T) \\ X_a(T) \end{pmatrix} = \begin{pmatrix} X_m \cos(\Omega T + \Phi_1) \\ X_{am} \cos(\Omega T + \Phi_2) \end{pmatrix}, \tag{18b}$$

the force transmissibility of the linear 1DOF and 2DOF vibration isolators is given by

$$G_{FL1} = \frac{\sqrt{X_m^2 + (2\zeta\Omega X_m)^2}}{F_e}, \tag{19a}$$

$$G_{FL2} = \frac{\sqrt{\beta^2 X_{am}^2 + (2\sigma\zeta_2\Omega)^2 X_{am}^2}}{F_e}. \tag{19b}$$

As can be seen in Eq. (16b) and Eq. (19b), the dynamic response and force transmissibility of the linear 2DOF vibration isolator are greatly influenced by the stiffness ratio β and mass ratio σ. Now we consider the natural frequencies of the linear 2DOF vibration isolator, ω_1 and ω_2. Note that when selecting σ and β, we must ensure $v = \beta / (\beta - (1+\sigma)) > 0$ based on Eq. (15), and so $\beta > (1+\sigma)$. Using Eq. (15), as β approaches close to $(1+\sigma)$, v tends to infinity, and as β approaches to infinity, v tends to 1. For both cases, ω_1 tends to 1 and ω_2 is a very large value. The natural frequencies of the linear 2DOF vibration isolator for changing stiffness ratio β are shown in Fig. 5. A range of mass ratio σ up to 0.2 are shown, higher values are arguably unrealistic due to the increased mass of the linear 2DOF vibration isolator, which is in line with the arguments regarding mass ratios for tuned-mass-dampers for example. From Fig. 5, it can be seen that ω_1 is a little larger than 1 and ω_2 has a much large value. As the stiffness ratio β increases, ω_1 firstly increases and then decreases, while ω_2 does the reverse.

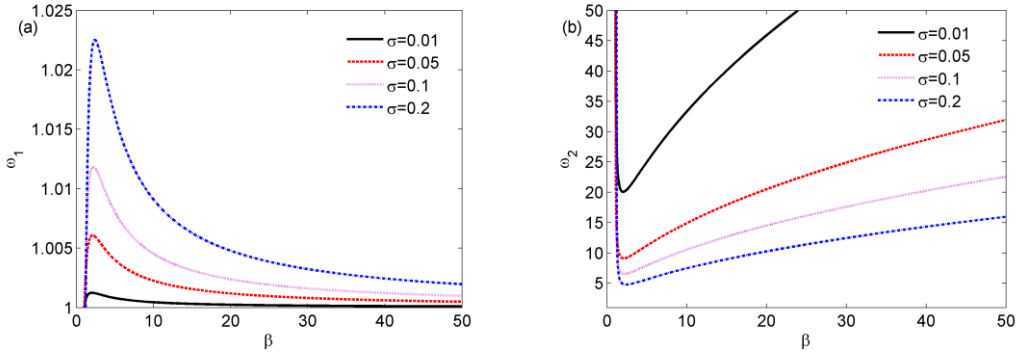

Fig. 5 (a) First and (b) second natural frequency of linear 2DOF vibration isolator for different β.

The dynamic response and force transmissibility of linear 1DOF and 2DOF vibration isolators for different β are shown in Fig. 6. As the stiffness ratio β increases, the peak dynamic displacement and peak force transmissibility of the linear 2DOF vibration isolator firstly increase and then decrease, the unity isolation frequency band remains almost the same. However the -40dB isolation frequency band firstly increases and then decreases. When the stiffness ratio β is selected such that ω_2 is mimimum ($\beta = 2.4$ in the case when $\sigma = 0.2$), the linear 2DOF vibration isolator has the largest -40dB isolation frequency band and meanwhile the peak dynamic displacement is not very large. When β increases to a large value, the peak dynamic displacement and peak force transmissibility of the linear 2DOF vibration isolator approach that of the linear 1DOF vibration isolator. For the linear 2DOF vibration isolator, when compared with the 1DOF linear vibration isolator, the peak dynamic displacement and peak force transmissibility are larger, the unity isolation frequency band is almost the same, while the force transmissibility in the higher isolation frequency band is smaller and the -40dB isolation frequency band can be larger.

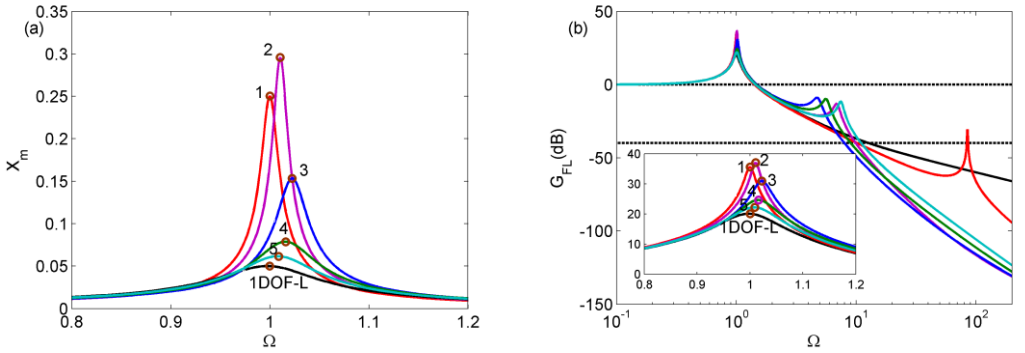

Fig. 6 (a) Dynamic response and (b) force transmissibility of linear 1DOF and 2DOF vibration isolators for different β with $\sigma = 0.2$, $\zeta = \zeta_1 = \zeta_2 = 0.05$ and $F_e = 0.005$.

Curve 1: $\beta = 1.201$; Curve 2: $\beta = 1.4$; Curve 3: $\beta = 2.4$; Curve 4: $\beta = 5$; Curve 5: $\beta = 10$.

The dynamic response and force transmissibility of linear 1DOF and 2DOF vibration

isolators for different σ are shown in Fig. 7. For the linear 2DOF vibration isolator, as the mass ratio σ increases, such that ω_1 increases while ω_2 decreases, the peak dynamic displacement, peak force transmissibility and unity isolation frequency band remain largely unaltered, however the -40dB isolation frequency band increases. As mentioned above, the mass ratio σ should not be too large, so in the following section, when analysing the isolation performance of the nonlinear 2DOF vibration isolator, the mass ratio σ is taken to be 0.2.

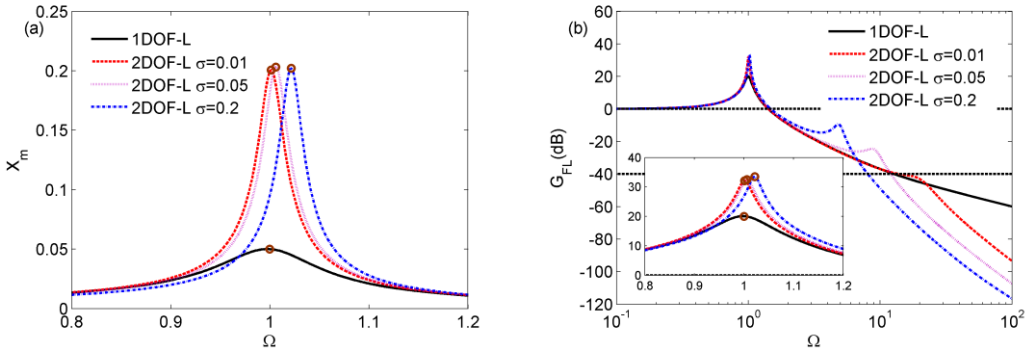

Fig. 7 (a) Dynamic response and (b) force transmissibility of linear 1DOF and 2DOF vibration isolators for different σ with $\beta = 2$, $\zeta = \zeta_1 = \zeta_2 = 0.05$ and $F_e = 0.005$.

Overall, when the static displacement of linear 1DOF and 2DOF vibration isolators is the same, the linear 2DOF vibration isolator can achieve a better isolation performance in the higher isolation frequency band (the -40dB isolation frequency band is larger) compared with the linear 1DOF vibration isolator. Meanwhile, the unity isolation frequency band is almost the same, but the peak dynamic displacement and peak force transmissibility increase.

Based on the above analysis, it can be seen that compared with the linear 1DOF vibration isolator, the linear 2DOF vibration isolator can have a larger -40dB isolation frequency band and the 1DOF QZS vibration isolator can have a smaller peak force transmissibility and a larger unity isolation frequency band. The following section investigates the dynamic response and force transmissibility of the nonlinear 2DOF vibration isolators to see whether they can achieve a better isolation performance in the higher isolation frequency band, while also having a smaller peak force transmissibility and a larger unity isolation frequency band.

4 The nonlinear 2DOF vibration isolator

Three different configurations for the nonlinear 2DOF vibration isolator shown in Fig. 8 are considered in this section. The nonlinearity is introduced using lateral springs at both degrees of freedom; as with the 1DOF QZS vibration isolator, these lateral springs are adjusted to be horizontal at the static equilibrium position. The three models arise

from different cases regarding where these lateral springs are attached, and are denoted as grounded-grounded (GG) Model, bottom-springs grounded (BG) Model and top-springs grounded (TG) Model. The GG Model and BG Model are considered in [29] and [30], respectively. In order to simplify the structure, the initial length of all these lateral springs is l_0 and the length when they are in the horizontal position, the static equilibrium position, is l. The other structure parameters are the same as those for the linear 2DOF vibration isolator in Section 3.

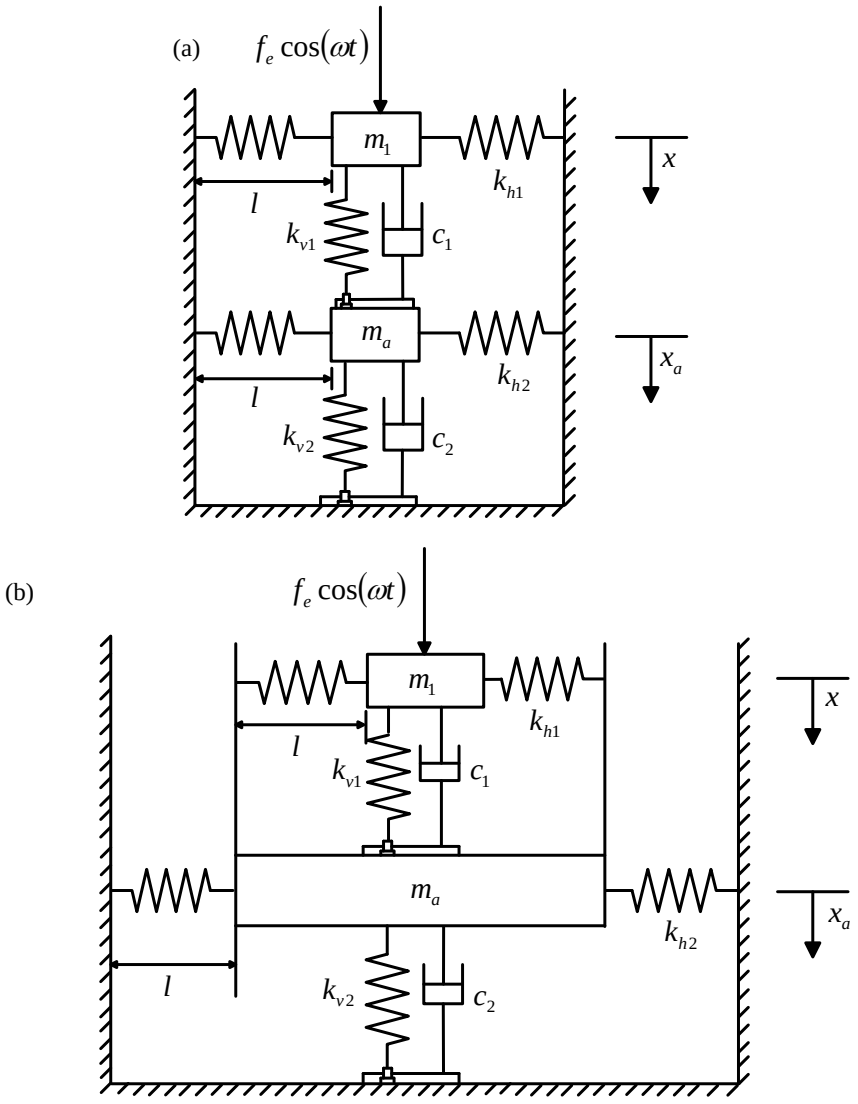

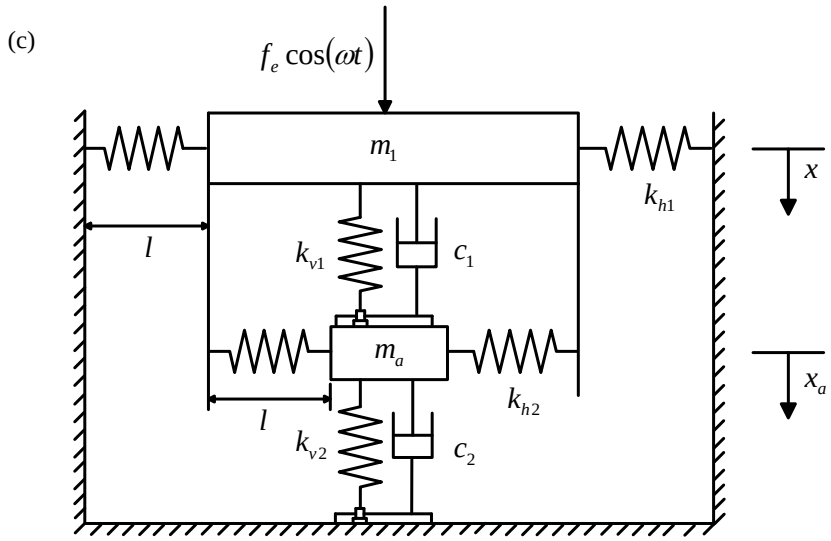

Fig. 8 Three kinds of nonlinear 2DOF vibration isolators at the static equilibrium position: Grounded-Grounded (GG) Model, (b) Bottom-springs Grounded (BG) Model, (c) Top-springs Grounded (TG) Model.

This section presents the dynamic equation of the BG Model as well as its dynamic response and force transmissibility. The analysis for the other two models is similar and has been included in Appendix A. This section also presents a detailed process for finding the best structural parameter sets for the BG Model according to the four performance indexes. The analysis process for the other two models is the same, so only the results are shown for brevity.

The dynamic equation of the BG Model under force excitation at the static equilibrium position is given by

$$m_1\ddot{x}+c_1(\dot{x}-\dot{x}_a)+\left(k_{v1}+2k_{h1}\left(1-\frac{l_0}{\sqrt{l^2+(x-x_a)^2}}\right)\right)(x-x_a)=f_e\cos(\omega t), \tag{20a}$$

$$\begin{aligned} &m_a\ddot{x}_a-c_1\dot{x}+(c_1+c_2)\dot{x}_a+\left(k_{v1}+2k_{h1}\left(1-\frac{l_0}{\sqrt{l^2+(x_a-x)^2}}\right)\right)(x_a-x)\\ &+\left(k_{v2}+2k_{h2}\left(1-\frac{l_0}{\sqrt{l^2+x_a^2}}\right)\right)x_a=0 \end{aligned}. \tag{20b}$$

Since the vertical springs are adjusted such that the lateral springs are horizontal at the static equilibrium position, the static displacement of the three nonlinear 2DOF vibration isolators is the same as for the linear 2DOF vibration isolator, namely m_1g/k_v, and results in the condition given in Eq. (15). Using Eq. (3), the non-dimensional parameters used here are defined as

$$K_1=\frac{k_{h1}}{k_v},\ K_2=\frac{k_{h2}}{k_v},\ \alpha_1=\nu-2K_1\frac{1-L}{L},\ \alpha_2=\beta-2K_2\frac{1-L}{L},\ \gamma_1=\frac{K_1}{U^2L^3},\ \gamma_2=\frac{K_2}{U^2L^3}. \tag{21}$$

In defining the non-dimensional parameters, we ensure that direct comparisons may be made with the 1DOF results. When the displacement of mass m_1 and m_a is small, the spring forces in Eq. (20) can be expanded as a Taylor series expansion at the corresponding static equilibrium positions of mass m_1 and m_a, such that

$$m_1\ddot{x}+c_1(\dot{x}-\dot{x}_a)+k_v\alpha_1(x-x_a)+\frac{k_v\gamma_1}{x_s^2}(x-x_a)^3=f_e\cos(\omega t), \tag{22a}$$

$$m_a\ddot{x}_a-c_1\dot{x}+(c_1+c_2)\dot{x}_a+k_v\alpha_1(x_a-x)+\frac{k_v\gamma_1}{x_s^2}(x_a-x)^3+k_v\alpha_2x_a+\frac{k_v\gamma_2}{x_s^2}x_a^3=0. \tag{22b}$$

This can be written in non-dimensional form as

$$\begin{bmatrix}1 & 0\\ 0 & \sigma\end{bmatrix}\begin{pmatrix}X''\\ X_a''\end{pmatrix}+\begin{bmatrix}2\zeta_1 & -2\zeta_1\\ -2\zeta_1 & 2\zeta_1+2\sigma\zeta_2\end{bmatrix}\begin{pmatrix}X'\\ X_a'\end{pmatrix}+\begin{bmatrix}\alpha_1 & -\alpha_1\\ -\alpha_1 & \alpha_1+\alpha_2\end{bmatrix}\begin{pmatrix}X\\ X_a\end{pmatrix}+\begin{bmatrix}\gamma_1 & 0\\ -\gamma_1 & \gamma_2\end{bmatrix}\begin{pmatrix}(X-X_a)^3\\ X_a^3\end{pmatrix}=\begin{pmatrix}F_e\cos(\Omega T)\\ 0\end{pmatrix}, \tag{23}$$

where the non-dimensional parameters are defined in Eqs. (3), (9), (17) and (21).

In the case of the 1DOF QZS vibration isolator, the QZS characteristic is achieved by setting $\alpha=0$, which means the natural frequency of the corresponding equivalent linear system is zero. Similarly, for the BG Model, we set the first natural frequency of the corresponding equivalent linear system to zero, $\omega_{n1}=0$, giving the condition $\alpha_1\alpha_2=0$. The resulting second natural frequency of the corresponding equivalent linear system, ω_{n2}, can be expressed as

$$\omega_{n2}=\sqrt{\alpha_1+\frac{\alpha_1+\alpha_2}{\sigma}}. \tag{24}$$

To satisfy $\alpha_1\alpha_2=0$ and hence achieve the QZS characteristic requires

$$L_{QZS}=\max\left\{\frac{2K_1}{\nu+2K_1},\ \frac{2K_2}{\beta+2K_2}\right\},\qquad K_{2QZS}=\frac{\beta L}{2(1-L)},$$

$$\beta_{QZS}=\max\left\{\frac{2K_1(1-L)(1+\sigma)}{2K_1(1-L)-1},\ 2K_2\frac{1-L}{L}\right\}. \tag{25}$$

Alongside these, to keep $\omega_{n2}\geq 0$ requires $L\geq L_{QZS}$, $K_2\leq K_{2QZS}$, $\beta\geq\beta_{QZS}$ and in addition to ensure $\nu>0$, $\beta_{QZS}\geq 1+\sigma$ is required based on Eq. (15).

Now we concentrate on the structural parameter sets of the length ratio L and stiffness ratios K_1 and K_2 with the stiffness ratio $\beta=k_{v2}/k$ set to 2. The length ratio L_{QZS} and ω_{n2} of the BG Model for different K_2 are shown in Fig. 9. As the stiffness ratio K_2 increases, the length ratio L_{QZS} firstly remains a constant value and then increases, while ω_{n2} firstly decreases and then increases. As can be seen in Fig. 9, a turning point exists where $\omega_{n2}=0$, when $L=L_{QZS}$ and $K_1/K_2=\nu/\beta$.

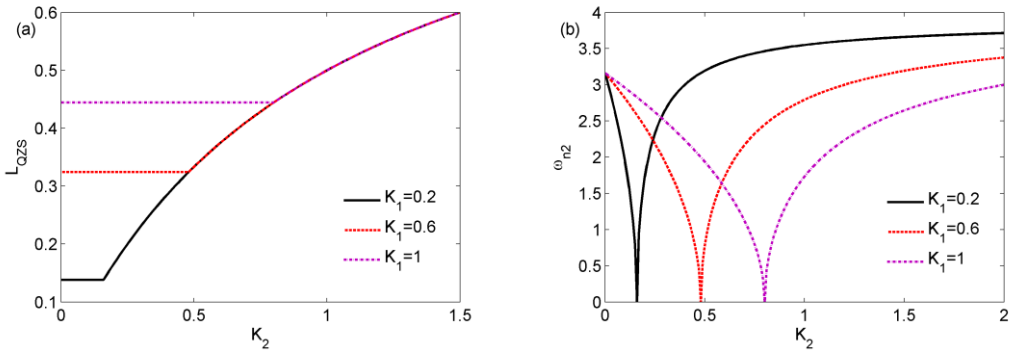

Fig. 9 (a) Length ratio L_{QZS} and (b) ω_{n2} of BG Model for different K_2 with $\sigma=0.2$, $U=2$ and $\beta=2$.

Then the HBM is used to obtain the steady state response of the BG Model, neglecting higher order harmonics, the approximate solutions of Eq. (23) are assumed to be the same forms as Eq. (18b). Note that the accuracy of the HBM approximate results is checked against numerical simulation results later, see Fig. 14. The resulting amplitude-frequency relationships can be obtained as

$$\left(\mathbf{K_1}-\Omega^2\mathbf{M}\right)\mathbf{X\Phi}-\Omega\left(\mathbf{CX\Phi}\right)\mathbf{A}+\frac{3}{4}\mathbf{K_3}\mathbf{X}^{(3\text{-}1)}\mathbf{\Phi}+\frac{3}{4}\mathbf{K_3}\mathbf{X}^{(3\text{-}2)}\mathbf{\Phi A}=\mathbf{F_e}, \tag{26}$$

where $\mathbf{M}=\begin{bmatrix}1 & 0\\ 0 & \sigma\end{bmatrix}$, $\mathbf{C}=\begin{bmatrix}2\zeta_1 & -2\zeta_1\\ -2\zeta_1 & 2\zeta_1+2\sigma\zeta_2\end{bmatrix}$, $\mathbf{K_1}=\begin{bmatrix}\alpha_1 & -\alpha_1\\ -\alpha_1 & \alpha_1+\alpha_2\end{bmatrix}$,

$\mathbf{K_3}=\begin{bmatrix}\gamma_1 & 0\\ -\gamma_1 & \gamma_2\end{bmatrix}$, $\mathbf{X}=\begin{bmatrix}X_m & 0\\ 0 & X_{am}\end{bmatrix}$, $\mathbf{\Phi}=\begin{bmatrix}\cos\Phi_1 & \sin\Phi_1\\ \cos\Phi_2 & \sin\Phi_2\end{bmatrix}$, $\mathbf{A}=\begin{bmatrix}0 & -1\\ 1 & 0\end{bmatrix}$, $\mathbf{F_e}=\begin{bmatrix}F_e & 0\\ 0 & 0\end{bmatrix}$,

$$\mathbf{X}^{(3\text{-}1)}=\begin{bmatrix}X_m^3+2X_mX_{am}^2-X_m^2X_{am}\cos\left(\Phi_1-\Phi_2\right) & -X_{am}^3-2X_m^2X_{am}+X_mX_{am}^2\cos\left(\Phi_1-\Phi_2\right)\\ 0 & X_{am}^3\end{bmatrix},$$

$$\mathbf{X}^{(3\text{-}2)}=\begin{bmatrix}X_m^2X_{am}\sin\left(\Phi_1-\Phi_2\right) & X_mX_{am}^2\sin\left(\Phi_1-\Phi_2\right)\\ 0 & 0\end{bmatrix}.$$

For a given excitation frequency Ω, the amplitudes X_m and X_{am}, phases Φ_1 and Φ_2 are obtained by solving four coupled nonlinear equations in Eq. (26) numerically. The transmitted force is given as $F_t=2\sigma\zeta_2X_a'+\alpha_2X_a+\gamma_2X_a^3$, from which, the force transmissibility can be obtained as

$$G_{FN2}=\frac{\sqrt{\left(2\sigma\zeta_2\Omega X_{am}\right)^2+\left(\alpha_2X_{am}+\frac{3}{4}\gamma_2X_{am}^3\right)^2}}{F_e}. \tag{27}$$

Unlike the 1DOF QZS vibration isolator, it is difficult to determine the peak dynamic displacement of the BG Model from Eq. (26), but it can be obtained using backbone curve analysis and energy balancing method. The backbone curves describe the fundamental characteristic of a vibration system which is undamped and unforced, and the energy balancing method relates the backbone curves to specific forced responses [32]. By setting $\zeta_1=\zeta_2=0$, $F_e=0$ and hence with $\sin\left(\Phi_2-\Phi_1\right)=0$ in Eq. (26), the backbone curves of the BG Model can be obtained. The energy balancing

method is based on the concept that for a steady state response, the total energy transfer of a vibration system due to the damping and forcing terms must be zero over one period of motion. For a detailed description of the energy balancing method, see [32,33]. Balancing the energy of the BG Model over a period of motion gives

$$\begin{aligned}&\int_0^{T_1}\left(X''+2\zeta_1X'-2\zeta_1X_a'+\alpha_1X-\alpha_1X_a+\gamma_1(X-X_a)^3\right)X'dT\\&+\int_0^{T_1}\left(\sigma X_a''-2\zeta_1X'+(2\zeta_1+2\sigma\zeta_2)X_a'-\alpha_1X+(\alpha_1+\alpha_2)X_a-\gamma_1(X-X_a)^3+\gamma_2X_a^3\right)X_a'dT\,,\\&=\int_0^{T_1}\left(F_e\cos(\Omega T)\right)X'dT\end{aligned}\qquad(28)$$

where T_1 is the period of the motion. Substituting Eq. (18b) into Eq. (28) gives

$$\zeta_1\Omega^2X_m^2+(\zeta_1+\sigma\zeta_2)\Omega^2X_{am}^2-2\zeta_1\Omega^2X_mX_{am}\cos(\Phi_1-\Phi_2)=-\frac{\Omega X_mF_e}{2}\sin\Phi_1\,.\qquad(29)$$

Using the condition $\sin(\Phi_2-\Phi_1)=0$ and assuming $\Phi_1=-\frac{\pi}{2}$, the peak dynamic displacement of the BG Model can be determined from the following sets of equations

$$\begin{cases}\pm\frac{3}{4}\gamma_1X_m^3-\frac{9}{4}\gamma_1X_{am}X_m^2\pm\left(\alpha_1-\Omega^2+\frac{9}{4}\gamma_1X_{am}^2\right)X_m-\alpha_1X_{am}-\frac{3}{4}\gamma_1X_{am}^3=0\\\left(\frac{3}{4}\gamma_1+\frac{3}{4}\gamma_2\right)X_{am}^3\mp\frac{9}{4}\gamma_1X_mX_{am}^2+\left(\alpha_1+\alpha_2-\sigma\Omega^2+\frac{9}{4}\gamma_1X_m^2\right)X_{am}\mp\left(\alpha_1X_m+\frac{3}{4}\gamma_1X_m^3\right)=0\\\zeta_1\Omega^2X_m^2+(\zeta_1+\sigma\zeta_2)\Omega^2X_{am}^2\mp2\zeta_1\Omega^2X_mX_{am}=\frac{\Omega X_mF_e}{2}\end{cases}\qquad(30)$$

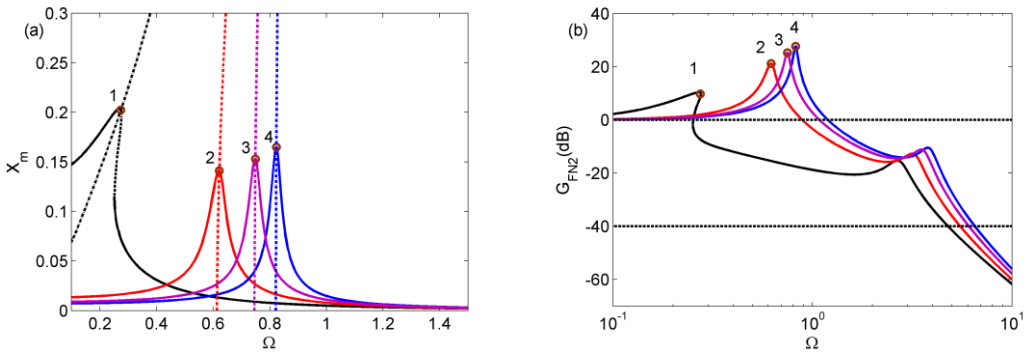

Fig. 10 (a) Dynamic response and (b) force transmissibility of BG Model for different L with $\sigma=0.2$, $U=2$, $\beta=2$, $K_1=1$, $K_2=0.2$, $\zeta_1=\zeta_2=0.05$ and $F_e=0.005$.

Curve 1: $L=L_{QZS}=4/9$; Curve 2: $L=0.5$; Curve 3: $L=0.55$; Curve 4: $L=0.6$.

The dynamic response and force transmissibility of the BG Model for different L are shown in Fig. 10. Note that the dynamic response around the second resonance in Fig. 10 and the subsequent plots is not shown as it is much smaller than that around the first resonance. When $L=L_{QZS}$, $\omega_{n1}=0$, as the spring length ratio L decreases, both ω_{n1} and ω_{n2} decrease, the peak force transmissibility decrease, the unity isolation frequency band and -40dB isolation frequency band increase, the peak dynamic displacement increases but arguably remains reasonable, so in this case, when $L=L_{QZS}$, the BG Model achieves better isolation performance. Equally it can be shown that if the

stiffness ratio K_2 varies, the BG Model has the largest -40dB isolation frequency band with $K_2 = K_{2QZS}$. In a practical vibration isolator [15, 16], it is convenient to change the spring length ratio L by using the spring deflection adjustment device for given vertical and lateral springs, whereas altering K_2 is inconvenient. So in the following analysis, the L_{QZS} case is considered and the stiffness ratio K_1 and K_2 are selected form the sets $K_1 \in [0 \quad 1]$ and $K_2 \in [0 \quad 1]$ respectively.

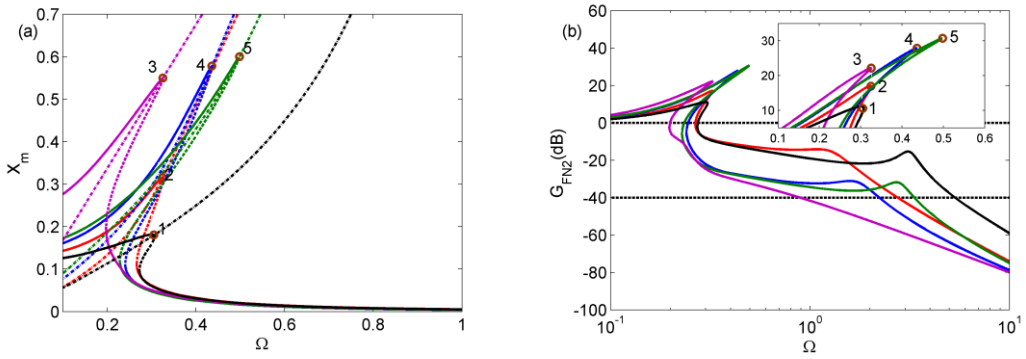

Fig. 11 (a) Dynamic response and (b) force transmissibility of BG Model for different K_2 when $L = L_{QZS}$ with $\sigma = 0.2$, $U = 2$, $\beta = 2$, $K_1 = 0.6$, $\zeta_1 = \zeta_2 = 0.05$ and $F_e = 0.005$.

Curve 1: $K_2 = 0$; Curve 2: $K_2 = 0.4$; Curve 3: $K_2 = 0.48$; Curve 4: $K_2 = 0.6$;

Curve 5: $K_2 = 1$.

Fig. 11 shows the dynamic response and force transmissibility of the BG Model for a range of K_2 with $K_1 = 0.6$ and $L = L_{QZS}$ selected such that $\omega_{n1} = 0$. It can be seen that increasing K_2 results in a significantly larger peak dynamic displacement and peak force transmissibility. It also affects the isolation frequency band, the unity isolation frequency band decreases and the -40dB isolation frequency band firstly increases and then decreases. The BG Model has the largest -40dB isolation frequency band when $K_2 = 0.48$, corresponding to $K_2 = (\beta / \nu) K_1$ such that $\omega_{n2} = 0$. When K_1 is fixed and K_2 varies, the trends are similar. So to improve the isolation performance of BG Model considering the first three performance indexes (Peak dynamic displacement, Peak transmissibility and Unity isolation frequency band), a small stiffness ratio K_2 should be selected, whereas when considering to increase the -40dB isolation frequency band, the stiffness ratio $K_2 = (\beta / \nu) K_1$ should be selected to ensure $\omega_{n2} = 0$.

Fig. 12 shows the dynamic response and force transmissibility of the BG Model for a range of K_1 with $K_2 = 0.6$ and $L = L_{QZS}$ selected such that $\omega_{n1} = 0$. It can be seen that increasing K_1 results in a significantly smaller peak dynamic displacement and peak force transmissibility, the unity isolation frequency band increases and the -40dB isolation frequency band firstly increases and then decreases. The BG Model has the largest -40dB isolation frequency band when $K_1 = 0.75$, corresponding to $K_1 = (\nu / \beta) K_2$ such that $\omega_{n2} = 0$. When K_2 is fixed and K_1 varies, the trends are similar. So to

improve the isolation performance of BG Model considering the first three performance indexes, a large stiffness ratio K_1 should be selected, whereas when considering to increase the -40dB isolation frequency band, the stiffness ratio $K_1=(\nu/\beta)K_2$ should be selected to ensure $\omega_{n2}=0$.

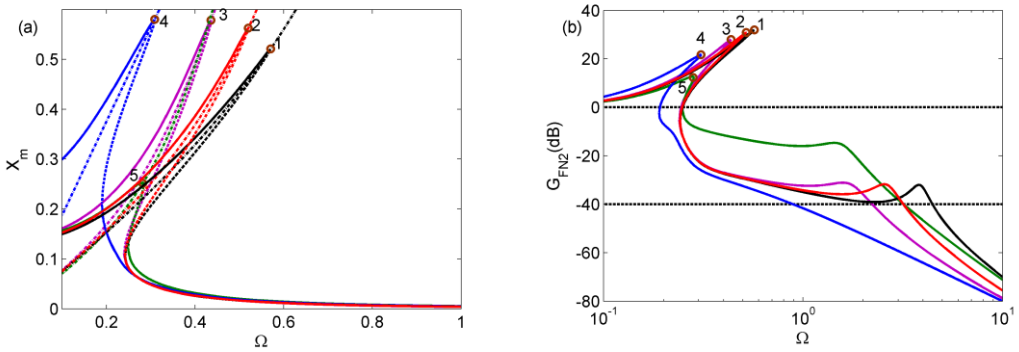

Fig. 12 (a) Dynamic response and (b) force transmissibility of BG Model for different K_1 when $L=L_{QZS}$ with $\sigma=0.2$, $U=2$, $\beta=2$, $K_2=0.6$, $\zeta_1=\zeta_2=0.05$ and $F_e=0.005$.

Curve 1: $K_1=0$; Curve 2: $K_1=0.4$; Curve 3: $K_1=0.6$; Curve 4: $K_1=0.75$;

Curve 5: $K_1=1$.

Using these results and concentrating on the -40dB isolation frequency band, Fig. 13 shows the dynamic response and force transmissibility of the BG Model for a range of K_1 with $K_2=(\beta/\nu)K_1$ and $L=L_{QZS}$ selected such that $\omega_{n1}=0$ and $\omega_{n2}=0$. It can be seen that increasing K_1 results in an increase of the peak dynamic displacement, however the peak force transmissibility decreases marginally and the unity isolation frequency band increases, the -40dB isolation frequency band remains almost the same. So considering the four performance indexes, a large stiffness ratio K_1 should be selected.

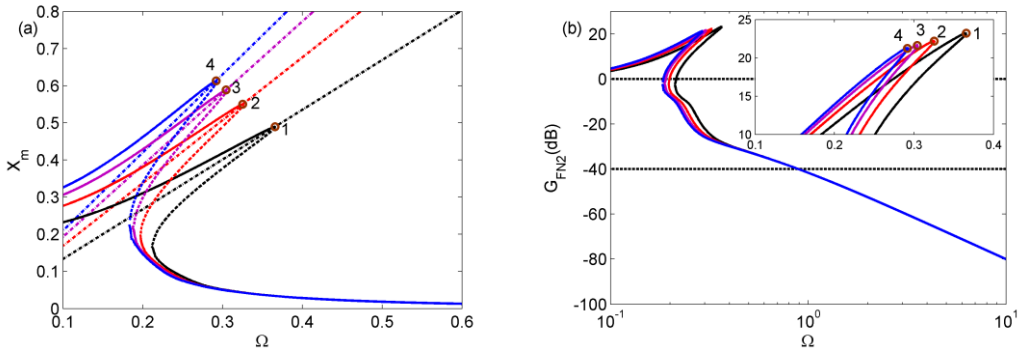

Fig. 13 (a) Dynamic response and (b) force transmissibility of BG Model for different K_1 when $L=L_{QZS}$ and $K_2=(\beta/\nu)K_1$ with $\sigma=0.2$, $U=2$, $\beta=2$, $\zeta_1=\zeta_2=0.05$ and $F_e=0.005$.

Curve 1: $K_1=0.4$; Curve 2: $K_1=0.6$; Curve 3: $K_1=0.8$; Curve 4: $K_1=1$.

At this stage it is worth considering the validity of using a Taylor series expansion (see Eq. (22)) to approximate the spring forces (see Eq. (20)) and the assumption made in the HBM analysis that the higher order harmonics are negligible. A comparison between analytic and numerical results of the dynamic response of the BG Model is shown in Fig. 14. The numerical results are obtained by solving the non-dimensional dynamic equations of (I) the full BG Model and (II) the BG Model with the Taylor series expansion directly using the numerical continuation method [34]. It can be seen that the error between the two sets of numerical results is small, which suggests that the Taylor series expansion is a good approximation here. Below resonances, errors between the analytic results and the numerical results are observed as the HBM used in this paper concentrates on the primary resonance whereas the numerical results also include the superharmonic resonances. Also the peak dynamic displacement obtained by the HBM is slightly larger than that of the numerical result. However overall, the analytic results obtained using HBM are a good representation of the true responses.

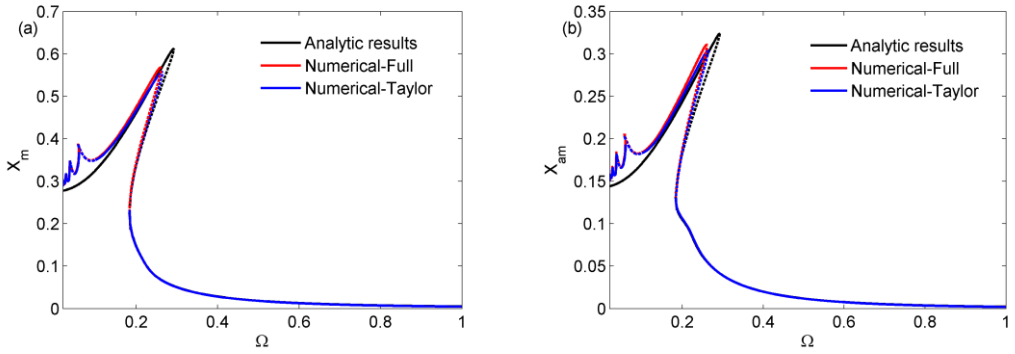

Fig. 14 Comparison between analytic results and numerical results of the dynamic response of BG Model with $\sigma = 0.2$, $K_1 = 1$, $K_2 = 0.8$, $L = L_{QZS}$, $U = 2$, $\beta = 2$, $\zeta_1 = \zeta_2 = 0.05$ and $F_e = 0.005$.

Overall, for BG Model with $L = L_{QZS}$, such that $\omega_{n1} = 0$, when considering the isolation performance based on the first three performance indexes, the stiffness ratio K_1 should be large (see Fig. 12) while the stiffness ratio K_2 should be small (see Fig. 11). Considering the structural parameter sets $K_1 \in [0 \quad 1]$ and $K_2 \in [0 \quad 1]$, $K_1 = 1$ and $K_2 = 0$ are selected, which indicates that the upper stage of the BG Model is nonlinear while the lower stage of the BG Model is linear. In contrast when considering to increase the -40dB isolation frequency band, $K_1 = 1$ and $K_2 = (\beta / v)K_1 = 0.8$ are selected for $\sigma = 0.2$ and $\beta = 2$ to ensure that $\omega_{n2} = 0$ (see Figs. 11, 12 and 13).

Following the similar analysis process, the best structural parameters selected in the sets $K_1 \in [0 \quad 1]$ and $K_2 \in [0 \quad 1]$ with $L = L_{QZS}$ for the GG and TG Models according to the four performance indexes can be obtained. Unlike the BG Model, when considering $L = L_{QZS}$, such that $\omega_{n1} = 0$, and choosing the stiffness ratio K_1 and K_2, ω_{2n} cannot be set to zero for the GG and TG Models. The equations for this analysis are given in

Appendix A. The outcomes are as follows:

GG Model: When considering the isolation performance based on the first three performance indexes, $K_1 = 1$ and $K_2 = 0$ are selected, which indicates that the upper stage of the GG Model is nonlinear while the lower stage of the GG Model is linear. When considering to increase the -40dB isolation frequency band, $K_1 = 0$ and $K_2 = 1$ are selected, which indicates that the upper stage of GG Model is linear while the lower stage of GG Model is nonlinear, this result is in accordance with the conclusions drawn in [29]. Lu *et al.* [29] concluded that the nonlinearity in the lower stage of GG Model has a profound performance effect and can significantly improve the isolation performance in the higher frequency band while nonlinearity in the upper stage has a minimal effect. However when $K_1 = 0$ and $K_2 = 1$ are selected, a larger peak dynamic displacement and peak force transmissibility and a decreased unity isolation frequency band are observed.

TG Model: $K_1 = 0$ and $K_2 = 1$ are selected which indicates that the upper stage of TG Model is linear while the lower stage of TG Model is nonlinear. In this configuration, the TG Model has a smaller peak dynamic displacement and peak force transmissibility and a larger unity and -40dB isolation frequency bands. Note that this configuration can be realized using the BG Model with $K_1 = 1$ and $K_2 = 0$ (compare Eq. (23) with Eq. (A.11)). So with the selected structural parameter sets, it follows that the TG Model is not helpful - its best configuration is matched by the BG Model and the BG Model can have better isolation performance for the -40dB isolation frequency band. We therefore disregard this model.

Finally the best structural parameter sets of the nonlinear 2DOF vibration isolators are summarised in Fig. 15, with the performance indexes given in Table 1. It can be seen that the -40dB isolation frequency band achieved by the BG Model with both $\omega_{n1} = 0$ and $\omega_{n2} = 0$ (Curve 1) is very good. However, this comes as the cost of a significantly larger peak dynamic displacement and peak force transmissibility. These can be reduced by using the BG Model with $K_1 = 1$ and $K_2 = 0$ (Curve 2), however the -40dB isolation frequency band is much worse. For completeness we show the two best structural parameter sets for the GG model, namely $K_1 = 0$ and $K_2 = 1$ (Curve 3) which gives good -40dB isolation frequency band and $K_1 = 1$ and $K_2 = 0$ (Curve 4) which gives good isolation performance for the first three performance indexes - however they are outperformed by the BG model results. We therefore disregard the GG Model, along with the TG Model as discussed above.

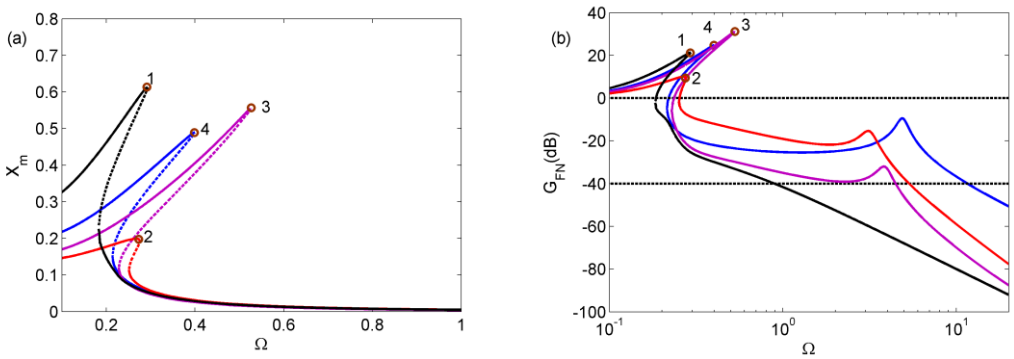

Fig. 15 Comparison of (a) dynamic response and (b) force transmissibility of the nonlinear 2DOF vibration isolators with $\sigma = 0.2$, $U = 2$, $\beta = 2$, $\zeta_1 = \zeta_2 = 0.05$ and $F_e = 0.005$.

Curve 1: BG Model, $K_1 = 1$, $K_2 = (\beta / \nu) K_1 = 0.8$, $L = L_{QZS} = 4/9$; Curve 2: BG Model, $K_1 = 1$, $K_2 = 0$, $L = L_{QZS} = 4/9$; Curve 3: GG Model, $K_1 = 0$, $K_2 = 1$, $L = L_{QZS} = 0.5$;

Curve 4: GG Model, $K_1 = 1$, $K_2 = 0$, $L = L_{QZS} = 0.6429$.

Table 1 The values of four performance indexes of the nonlinear 2DOF vibration isolators with $\sigma = 0.2$, $U = 2$, $\beta = 2$, $\zeta_1 = \zeta_2 = 0.05$ and $F_e = 0.005$.

Model	Peak dynamic displacement	Peak force Transmissibility /(dB)	Unity isolation frequency band	-40dB isolation frequency band
(1) BG Model $K_1 = 1, K_2 = 0.8$	0.6135	21.2527	>0.2918	>**0.8902**
(2) BG Model $K_1 = 1$, $K_2 = 0$	**0.1977**	**9.4456**	>**0.2729**	>5.336
(3) GG Model $K_1 = 0$, $K_2 = 1$	0.557	31.2302	>0.5269	>4.4476
(4) GG Model $K_1 = 1$, $K_2 = 0$	0.4889	24.7563	>0.3985	>11.5685

5 Discussion

A comparison of the dynamic response and force transmissibility for the four vibration isolators (the GG and TG models being disregarded) with best structural parameter sets according to the four performance indexes is shown in Fig. 16. The corresponding values for the four performance indexes are given in Table 2. Recall that we set the static displacement to be the same for each vibration isolator. We see that the linear 1DOF isolator (Curve 5) results in the minimum peak dynamic displacement. Adding lateral springs to give 1DOF QZS vibration isolator (Curve 6) allows the peak force transmissibility and the unity isolation frequency band to be improved significantly. In fact the 1DOF QZS vibration isolator has the smallest peak force transmissibility and

largest unity isolation frequency band across all the four vibration isolators. However this is at the cost of increasing the peak dynamic displacement compared with linear 1DOF vibration isolator.

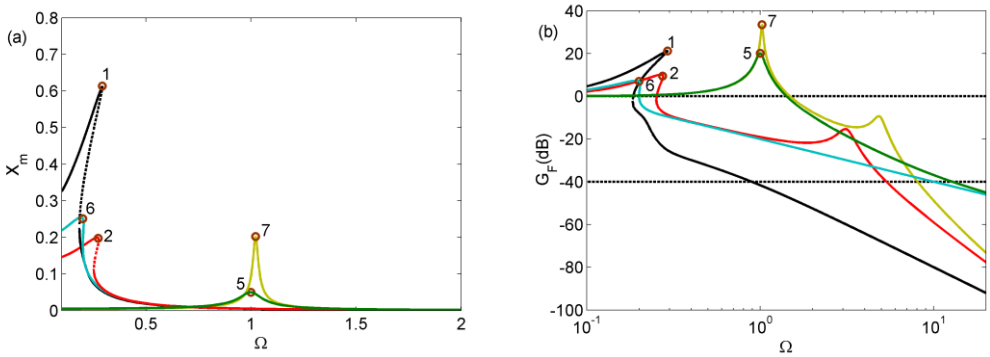

Fig. 16 Comparison of (a) dynamic response and (b) force transmissibility of four vibration isolators ($\sigma = 0.2$, $U = 2$, $\beta = 2$, $F_e = 0.005$, $\zeta_1 = \zeta_2 = 0.05$).

Curve 1: BG Model, $K_1 = 1$, $K_2 = (\beta / \nu) K_1 = 0.8$, $L = L_{QZS} = 4/9$; Curve 2: BG Model, $K_1 = 1$, $K_2 = 0$, $L = L_{QZS} = 4/9$; Curve 5: linear 1DOF vibration isolator; Curve 6: 1DOF QZS vibration isolator $K = 1$, $L = L_{QZS} = 2/3$; Curve 7: linear 2DOF vibration isolator.

Table 2 The values of four performance indexes of four vibration isolators with $\sigma = 0.2$, $U = 2$, $\beta = 2$, $\zeta_1 = \zeta_2 = 0.05$ and $F_e = 0.005$.

Model	Peak dynamic displacement	Peak force Transmissibility /(dB)	Unity isolation frequency band	-40dB isolation frequency band
(1) BG Model $K_1 = 1, K_2 = 0.8$	0.6135	21.2527	>0.2918	>**0.8902**
(2) BG Model $K_1 = 1$, $K_2 = 0$	0.1977	9.4456	>0.2729	>5.336
(5) 1DOF linear vibration isolator	**0.05**	20.0432	>1.4142	>12.7766
(6) 1DOF QZS vibration isolator	0.2507	**6.9701**	>**0.1994**	>9.9995
(7) linear 2DOF vibration isolator	0.2022	33.4678	>1.481	>8.0543

For linear and QZS 1DOF vibration isolators, the -40dB isolation frequency band is quite similar. To increase this requires a second degree of freedom. The linear 2DOF vibration isolator (Curve 7) increases the -40dB isolation frequency band, however at the cost of increased peak dynamic displacement and peak force transmissibility. To further increase the -40dB isolation frequency band requires the use of the BG Model with both

$\omega_{n1}=0$ and $\omega_{n2}=0$. Note however this configuration leads to a significantly larger peak dynamic displacement. We also observe that the BG Model with $K_1=1$ and $K_2=0$ gives a good isolation performance across all the four performance indexes, and that this configuration is simple: the upper stage is nonlinear while the lower stage is linear. For BG Model chosen for the four performance indexes, when compared with linear and QZS 1DOF vibration isolators, the -40dB isolation frequency band is larger; when compared with the linear 2DOF vibration isolator, the peak force transmissibility is smaller and the unity isolation frequency band is larger. Comparison of Table 2 reveal that the nonlinear 2DOF vibration isolators can give improved isolation performance for the -40dB isolation frequency band, however for the other performance indexes, a 1DOF vibration isolator is better.

6 Conclusions

This paper presents three kinds of nonlinear 2DOF vibration isolators with QZS characteristic and compares the isolation performance with linear and QZS 1DOF vibration isolators and a linear 2DOF vibration isolator. To ensure a fair comparison, the static displacement of each vibration isolator is the same. The isolation performance of the vibration isolator is evaluated using four performance indexes: peak dynamic displacement, peak transmissibility, unity isolation frequency band and -40dB isolation frequency band.

Firstly, the dynamic response and isolation performance of the 1DOF QZS vibration isolator is compared with the equivalent linear one. The results show that when the excitation force amplitude is small, the 1DOF QZS vibration isolator can have a smaller peak force transmissibility and a larger unity isolation frequency band, while the force transmissibility of both vibration isolators in the higher frequency band is almost the same, both reduce at a rate of 40dB/decade.

Then, the dynamic response and isolation performance of linear 2DOF vibration isolator is compared with the linear 1DOF vibration isolator. It is shown that the linear 2DOF vibration isolator can achieve a better isolation performance in the higher isolation frequency band, which the force transmissibility in the higher isolation frequency band reducing at a rate of 80dB/decade, and a larger -40dB isolation frequency band, with little change in the unity isolation frequency band. However the peak dynamic displacement and peak force transmissibility are larger.

Lastly, the dynamic response and isolation performance of three configurations of nonlinear 2DOF vibration isolators are compared with the linear and QZS 1DOF vibration isolators and the linear 2DOF vibration isolator. The best structural parameter sets of the nonlinear 2DOF vibration isolators based on the four performance indexes are identified. It is shown that when the excitation force amplitude is small, the nonlinear

2DOF vibration isolators have both larger unity and -40dB isolation frequency bands and a smaller peak force transmissibility while the peak dynamic displacement is not very large. The BG Model has the best isolation performance over the three kinds of nonlinear 2DOF vibration isolators. When considering to minimize peak force transmissibility and increase unity isolation frequency band, the 1DOF QZS vibration isolator should be chosen; when considering a good isolation performance across all the four performance indexes, arguably the BG Model based on the first three performance indexes should be chosen; if instead the maximization of the -40dB isolation frequency band is considered, the BG Model with $\omega_{n1}=\omega_{n2}=0$ should be chosen. Finally if the peak dynamic displacement is the only considered important criterion, a simple linear 1DOF vibration isolator is sufficient.

Acknowledgments

The research described in this paper is supported by the Fundamental Research Funds for the Central Universities (Grant no. NZ2015103) and the open project of State Key Laboratory for Strength and Vibration of Mechanical Structures (Grant no. SV2015-KF-01). In addition, Yong Wang is supported as a visiting doctoral student at the University of Bristol by the Chinese Scholarship Council (Grant no. 201506830023) and Simon A. Neild is supported by the EPSRC Fellowship EP/K005375/1.

Appendix A

A.1 The GG Model

The dynamic equation of the GG Model under force excitation at the static equilibrium position is given by

$$m_1\ddot{x}+c_1\left(\dot{x}-\dot{x}_a\right)+\left(k_{v1}+2k_{h1}\left(1-\frac{l_0}{\sqrt{l^2+x^2}}\right)\right)x-k_{v1}x_a=f_e\cos\left(\omega t\right), \tag{A.1a}$$

$$m_a\ddot{x}_a-c_1\dot{x}+\left(c_1+c_2\right)\dot{x}_a-k_{v1}x+k_{v1}x_a+\left(k_{v2}+2k_{h2}\left(1-\frac{l_0}{\sqrt{l^2+x_a^2}}\right)\right)x_a=0. \tag{A.1b}$$

Using a Taylor series expansion, Eq. (A.1) can be approximated as

$$m_1\ddot{x}+c_1\left(\dot{x}-\dot{x}_a\right)+k_v\alpha_1 x+\frac{k_v\gamma_1}{x_s^2}x^3-k_v v x_a=f_e\cos\left(\omega t\right), \tag{A.2a}$$

$$m_a\ddot{x}_a-c_1\dot{x}+\left(c_1+c_2\right)\dot{x}_a-k_v v x+k_v\left(v+\alpha_2\right)x_a+\frac{k_v\gamma_2}{x_s^2}x_a^3=0. \tag{A.2b}$$

Following the same non-dimensional procedure described in Section 4, Eq. (A.2) can be written as

$$\begin{bmatrix}1 & 0\\ 0 & \sigma\end{bmatrix}\begin{pmatrix}X''\\ X_a''\end{pmatrix}+\begin{bmatrix}2\zeta_1 & -2\zeta_1\\ -2\zeta_1 & 2\zeta_1+2\sigma\zeta_2\end{bmatrix}\begin{pmatrix}X'\\ X_a'\end{pmatrix}$$
$$+\begin{bmatrix}\alpha_1 & -v\\ -v & v+\alpha_2\end{bmatrix}\begin{pmatrix}X\\ X_a\end{pmatrix}+\begin{bmatrix}\gamma_1 & 0\\ 0 & \gamma_2\end{bmatrix}\begin{pmatrix}X^3\\ X_a^3\end{pmatrix}=\begin{pmatrix}F_e\cos(\Omega T)\\ 0\end{pmatrix}. \quad (A.3)$$

The resulting amplitude-frequency relationships of the GG Model can be obtained

$$\left(\mathbf{K_1}-\Omega^2\mathbf{M}\right)\mathbf{X\Phi}-\Omega\left(\mathbf{CX\Phi}\right)\mathbf{A}+\frac{3}{4}\mathbf{K_3X^{(3)}\Phi}=\mathbf{F_e}, \quad (A.4)$$

where $\mathbf{K_1}=\begin{bmatrix}\alpha_1 & -v\\ -v & v+\alpha_2\end{bmatrix}$, $\mathbf{K_3}=\begin{bmatrix}\gamma_1 & 0\\ 0 & \gamma_2\end{bmatrix}$, $\mathbf{X^{(3)}}=\begin{bmatrix}X_m^3 & 0\\ 0 & X_{am}^3\end{bmatrix}$, the other parameters in Eq. (A.4) are the same with the parameters shown in Section 4.

The transmitted force of the GG Model is given as

$$\begin{aligned}F_t&=2\sigma\zeta_2X_a'+(\alpha_1-v)X+\gamma_1X^3+\alpha_2X_a+\gamma_2X_a^3\\&=\mathbf{C_t}\begin{pmatrix}X'\\ X_a'\end{pmatrix}+\mathbf{K_{t1}}\begin{pmatrix}X\\ X_a\end{pmatrix}+\mathbf{K_{t3}}\begin{pmatrix}X^3\\ X_a^3\end{pmatrix}\end{aligned}, \quad (A.5)$$

where $\mathbf{C_t}=\begin{bmatrix}0 & 2\sigma\zeta_2\end{bmatrix}$, $\mathbf{K_{t1}}=\begin{bmatrix}\alpha_1-v & \alpha_2\end{bmatrix}$ and $\mathbf{K_{t3}}=\begin{bmatrix}\gamma_1 & \gamma_2\end{bmatrix}$.

Using Eq. (A.4) and Eq. (A.5), the amplitude of the force is written as

$$F_{t1}\mathbf{\Phi_t}=\mathbf{K_{t1}X\Phi}+\frac{3}{4}\mathbf{K_{t3}X^{(3)}\Phi}-\Omega\left(\mathbf{C_tX\Phi}\right)\mathbf{A}, \quad (A.6)$$

where $\mathbf{\Phi_t}=\begin{bmatrix}\cos\Phi_t & \sin\Phi_t\end{bmatrix}$. The force transmissibility of the GG Model can be obtained

$$G_{FN1}=\frac{F_{t1}}{F_e}. \quad (A.7)$$

Finally, using the backbone curve analysis and energy balancing method described in Section 4, the peak dynamic displacement of the GG Model can be determined from the following sets of equations

$$\begin{cases}\frac{3}{4}\gamma_1X_m^3+\left(\alpha_1-\Omega^2\right)X_m\mp vX_{am}=0\\ \frac{3}{4}\gamma_2X_{am}^3+\left(v+\alpha_2-\sigma\Omega^2\right)X_{am}\mp vX_m=0\\ \zeta_1\Omega^2X_m^2+\left(\zeta_1+\sigma\zeta_2\right)\Omega^2X_{am}^2\mp2\zeta_1\Omega^2X_mX_{am}=\frac{\Omega X_mF_e}{2}\end{cases}. \quad (A.8)$$

A.2 The TG Model

The dynamic equation of the TG Model under force excitation at the static equilibrium position is given by

$$\begin{aligned}&m\ddot{x}+c_1(\dot{x}-\dot{x}_a)+\left(k_{v1}+2k_{h1}\left(1-\frac{l_0}{\sqrt{l^2+x^2}}\right)\right)x-k_{v1}x_a\\&+2k_{h2}\left(1-\frac{l_0}{\sqrt{l^2+(x-x_a)^2}}\right)(x-x_a)=f_e\cos(\omega t)\end{aligned}, \quad (A.9a)$$

$$m_a\ddot{x}_a-c_1\dot{x}+(c_1+c_2)\dot{x}_a+k_{v1}(x_a-x)+k_{v2}x_a+2k_{h2}\left(1-\frac{l_0}{\sqrt{l^2+(x_a-x)^2}}\right)(x_a-x)=0. \quad (A.9b)$$

Using a Taylor series expansion, Eq. (A.9) can be approximated as

$$\begin{aligned} & m_1\ddot{x}+c_1(\dot{x}-\dot{x}_a)+k_v(\alpha_1+\alpha_2-\beta)x-k_v(v+\alpha_2-\beta)x_a \\ & +\frac{k_v\gamma_1}{x_s^2}x^3+\frac{k_v\gamma_2}{x_s^2}(x-x_a)^3=f_e\cos(\omega t) \end{aligned} \quad , \tag{A.10a}$$

$$m_a\ddot{x}_a-c_1\dot{x}+(c_1+c_2)\dot{x}_a-k_v(v+\alpha_2-\beta)x+k_v(v+\alpha_2)x_a+\frac{k_v\gamma_2}{x_s^2}(x_a-x)^3=0\,. \tag{A.10b}$$

Following the same non-dimensional procedure described in Section 4, Eq. (A.10) can be written as

$$\begin{aligned} & \begin{bmatrix}1 & 0\\ 0 & \sigma\end{bmatrix}\begin{pmatrix}X''\\ X_a''\end{pmatrix}+\begin{bmatrix}2\zeta_1 & -2\zeta_1\\ -2\zeta_1 & 2\zeta_1+2\sigma\zeta_2\end{bmatrix}\begin{pmatrix}X'\\ X_a'\end{pmatrix}+\begin{bmatrix}\alpha_1+\alpha_2-\beta & -(v+\alpha_2-\beta)\\ -(v+\alpha_2-\beta) & v+\alpha_2\end{bmatrix}\begin{pmatrix}X\\ X_a\end{pmatrix} \\ & +\begin{bmatrix}\gamma_1 & \gamma_2\\ 0 & -\gamma_2\end{bmatrix}\begin{pmatrix}X^3\\ (X-X_a)^3\end{pmatrix}=\begin{pmatrix}F_e\cos(\Omega T)\\ 0\end{pmatrix} \end{aligned}\,. \tag{A.11}$$

The resulting amplitude-frequency relationships of the TG Model can be obtained

$$(\mathbf{K_1}-\Omega^2\mathbf{M})\mathbf{X\Phi}-\Omega(\mathbf{CX\Phi})\mathbf{A}+\frac{3}{4}\mathbf{K_3}\mathbf{X^{(3\text{-}1)}\Phi}+\frac{3}{4}\mathbf{K_3}\mathbf{X^{(3\text{-}2)}\Phi A}=\mathbf{F_e}\,, \tag{A.12}$$

where $\mathbf{K_1}=\begin{bmatrix}\alpha_1+\alpha_2-\beta & -(v+\alpha_2-\beta)\\ -(v+\alpha_2-\beta) & v+\alpha_2\end{bmatrix}$, $\mathbf{K_3}=\begin{bmatrix}\gamma_1 & \gamma_2\\ 0 & -\gamma_2\end{bmatrix}$,

$$\mathbf{X^{(3\text{–}1)}}=\begin{bmatrix}X_m^3 & 0\\ X_m^3+2X_mX_{am}^2-X_m^2X_{am}\cos(\Phi_1-\Phi_2) & -X_{am}^3-2X_m^2X_{am}+X_mX_{am}^2\cos(\Phi_1-\Phi_2)\end{bmatrix},$$

$\mathbf{X^{(3\text{–}2)}}=\begin{bmatrix}0 & 0\\ X_m^2X_{am}\sin(\Phi_1-\Phi_2) & X_mX_{am}^2\sin(\Phi_1-\Phi_2)\end{bmatrix}$, the other parameters in Eq. (A.12) are the same with the parameters defined in Section 4.

The transmitted force of the TG Model is given as

$$\begin{aligned} F_t &= 2\sigma\zeta_2X_a'+(\alpha_1-v)X+\gamma_1X^3+\beta X_a \\ &= \mathbf{C_t}\begin{pmatrix}X'\\ X_a'\end{pmatrix}+\mathbf{K_{t1}}\begin{pmatrix}X\\ X_a\end{pmatrix}+\mathbf{K_{t3}}\begin{pmatrix}X^3\\ X_a^3\end{pmatrix} \end{aligned}\quad , \tag{A.13}$$

where $\mathbf{C_t}=[0\quad 2\sigma\zeta_2]$, $\mathbf{K_{t1}}=[\alpha_1-v\quad \beta]$ and $\mathbf{K_{t3}}=[\gamma_1\quad 0]$.

Using Eq. (A.12) and Eq. (A.13), the amplitude of the force is written as

$$F_{t3}\mathbf{\Phi_t}=\mathbf{K_{t1}X\Phi}+\frac{3}{4}\mathbf{K_{t3}X^{(3)}\Phi}-\Omega(\mathbf{C_tX\Phi})\mathbf{A}\,. \tag{A.14}$$

The force transmissibility of the TG Model can be obtained

$$G_{NF3}=\frac{F_{t3}}{F_e}\,. \tag{A.15}$$

Finally, using the backbone curve analysis and energy balancing method described in Section 4, the peak dynamic displacement of the TG Model can be determined from the following sets of equations

$$\begin{cases} \pm\left(\frac{3}{4}\gamma_1+\frac{3}{4}\gamma_2\right)X_m^3-\frac{9}{4}\gamma_2 X_{am}X_m^2\pm\left(\alpha_1+\alpha_2-\beta-\Omega^2+\frac{9}{4}\gamma_2 X_{am}^2\right)X_m \\ -\left(\nu+\alpha_2-\beta\right)X_{am}-\frac{3}{4}\gamma_2 X_{am}^3=0 \\ \frac{3}{4}\gamma_2 X_{am}^3\mp\frac{9}{4}\gamma_2 X_m X_{am}^2+\left(\nu+\alpha_2-\sigma\Omega^2+\frac{9}{4}\gamma_2 X_m^2\right)X_{am} \\ \mp\left(\left(\nu+\alpha_2-\beta\right)X_m+\frac{3}{4}\gamma_2 X_m^3\right)=0 \\ \zeta_1\Omega^2 X_m^2+\left(\zeta_1+\sigma\zeta_2\right)\Omega^2 X_{am}^2\mp 2\zeta_1\Omega^2 X_m X_{am}=\frac{\Omega X_m F_e}{2} \end{cases} . \quad \text{(A.16)}$$

References

[1] Harris, C.M., Piersol, A.G.: Shock and Vibration Handbook. McGraw-Hill, New York (2002)

[2] Ibrahim, R.A.: Recent advances in nonlinear passive vibration isolators. J. Sound Vib. **314**(3-5), 371-452 (2008)

[3] Alabuzhev, P., Gritchin, A., Kim, L., Migirenko, G., Chon, V., Stepanov, P.: Vibration protecting and measuring system with quasi-zero stiffness. Hemisphere Publishing, New York (1989)

[4] Carrella, A., Brennan, M.J., Waters, T.P.: Static analysis of a passive vibration isolator with quasi-zero-stiffness characteristic. J. Sound Vib. **301**(3-5), 678-689 (2007)

[5] Carrella, A., Brennan, M.J.,Waters, T.P., Lopes Jr.,V.: Force and displacement transmissibility of a nonlinear isolator with high-static-low-dynamic stiffness. Int. J. Mech. Sci. **55**(1), 22–29 (2012)

[6] Xu, D., Zhang, Y., Zhou, J., Lou, J.: On the analytical and experimental assessment of performance of a quasi-zero-stiffness isolator. J. Vib. Control (2013). doi: 10.1177/1077546313484049

[7] Le, T.D., Ahn, K.K.: A vibration isolation system in low frequency excitation region using negative stiffness structure for vehicle seat. J. Sound Vib. **330**(26), 6311–6335 (2011)

[8] Le, T.D., Ahn, K.K.: Experimental investigation of a vibration isolation system using negative stiffness structure. Int. J. Mech. Sci. **70**, 99–112 (2013)

[9] Le, T.D., Ahn, K.K.: Fuzzy sliding mode controller of a pneumatic active isolating system using negative stiffness structure. J. Mech. Sci. Technol. **26**(12), 3873-3884 (2012)

[10] Platus, D.L., Negative-stiffness-mechanism vibration isolation systems. In: Proceedings of SPIE's International Symposium on Optical Science, Engineering, and Instrumentation, pp. 98-105. (1999)

[11] Yang, J., Xiong, Y., Xing, J.: Dynamics and power flow behaviour of a nonlinear vibration isolation system with a negative stiffness mechanism. J. Sound Vib. **332**(1), 167-183 (2013)

[12] Liu, X., Huang, X., Hua, H.: On the characteristics of a quasi-zero stiffness isolator using Euler buckled beam as negative stiffness corrector. J. Sound Vib. **332**(14), 3359-3376 (2013)

[13] Huang, X., Liu, X., Sun, J., Zhang, Z., Hua, H.: Vibration isolation characteristics of a nonlinear isolator using Euler buckled beam as negative stiffness corrector: a theoretical and experimental study. J. Sound Vib. **333**(4), 1132-1148 (2014)

[14] Shaw, A.D., Neild, S.A., Wagg, D.J.: Dynamic analysis of high static low dynamic stiffness vibration isolation mounts. J. Sound Vib. **332** (6), 1437-1455 (2013)

[15] Shaw, A.D., Neild, S.A., Wagg, D.J., Weaver, P.M., Carrella, A.: A nonlinear spring mechanism incorporating a bistable composite plate for vibration isolation. J. Sound Vib. **332** (24), 6265–6275 (2013)

[16] Lan, C.C., Yang, S.A., Wu, Y.S.: Design and experiment of a compact quasi-zero-stiffness isolator capable of a wide range of loads. J. Sound Vib. **333** (20), 4843-4858 (2014)

[17] Zhou, J., Xu, D., Bishop, S.: A torsion quasi-zero stiffness vibration isolator. J. Sound Vib. **338**, 121-133 (2015)

[18] Zhou, J., Wang, X., Xu, D., Bishop, S.: Nonlinear dynamic characteristics of a quasi-zero stiffness vibration isolator with cam-roller-spring mechanisms. J. Sound Vib. **346**, 53-69 (2015)

[19] Liu, C., Jing, X.: Vibration energy harvesting with a nonlinear structure. Nonlinear Dyn. (2016). doi: 10.1007/s11071-016-2630-7

[20] Robertson, W.S., Kidner, M.R.F., Cazzolato, B.S., Zander, A.C.: Theoretical design parameters for a quasi-zero stiffness magnetic spring for vibration isolation. J. Sound Vib. **326** (1-2), 88-103 (2009)

[21] Zhou, N., Liu, K.: A tunable high-static low-dynamic stiffness vibration isolator. J. Sound Vib. **329** (9), 1254-1273 (2010)

[22] Xu, D., Yu, Q., Zhou, J., Bishop, S.: Theoretical and experimental analyses of a nonlinear magnetic vibration isolator with quasi-zero-stiffness characteristic. J. Sound Vib. **332** (14), 3377-3389 (2013)

[23] Huang, X., Liu, X., Sun, J., Zhang, Z., Hua, H.: Effect of the system imperfections on the dynamic response of a high-static-low-dynamic stiffness vibration isolator. Nonlinear Dyn. **76** (2), 1157-1167 (2014)

[24] Huang, X., Liu, X., Hua, H.: Effects of stiffness and load imperfection on the isolation performance of a high-static-low-dynamic-stiffness non-linear isolator under base displacement excitation. Int. J. Nonlinear Mech. **65**, 32-43 (2014)

[25] Shaw, A.D., Neild, S.A., Friswell, M.I.: Relieving the effect of static load errors in nonlinear vibration isolation mounts through stiffness asymmetries. J. Sound Vib. **339**, 84-98 (2015)

[26] Abolfathi, A., Brennan, M.J., Waters, T.P., Tang, B.: On the effects of mistuning a force-excited system containing a quasi-zero-stiffness vibration isolator. J. Vib. Acoust. **137** (4), 044502 (2015)

[27] Gorman, R.M.: Design and advantage of a two-stage mounting system for major machine in ships' engine room. Shock and Vibration Bulletin 35 (1966).

[28] Wang, Y., Chen, C.G., Hua, H.X., Shen, R.Y.: Optimal design of ship floating raft system power equipment. Shipbuilding of China **42** (1), 45-49 (2001)

[29] Lu, Z., Brennan, M.J., Yang, T., Li, X., Liu, Z.: An investigation of a two-stage nonlinear vibration isolation system. J. Sound Vib. **332** (3), 1456-1464 (2013)

[30] Lu, Z., Yang, T., Brennan, M.J., Li, X., Liu, Z.: On the Performance of a Two-stage Vibration Isolation System which has Geometrically Nonlinear Stiffness. J. Vib. Acoust. **136**(6), 064501 (2014)

[31] Wagg, D.J., Neild, S.A.: Nonlinear Vibration with Control. Springer, New York (2009)

[32] Hill, T.L., Cammarano, A., Neild, S.A., Wagg, D.J.: An analytical method for the optimisation of weakly nonlinear systems. Proceedings of EURODYN (2014) 1981-1988.

[33] Hill, T.L., Cammarano, A., Neild, S.A., Wagg, D.J.: Interpreting the forced responses of a two-degree-of-freedom nonlinear oscillator using backbone curves. J. Sound Vib. **349**, 276-288 (2015)

[34] Peeters, M., Viguié, R., Sérandour, G., Kerschen, G., Golinval, J.C.: Nonlinear normal modes, Part II: Toward a practical computation using numerical continuation techniques. Mech. Syst. Signal Process. **23**(1), 195-216 (2009)